

CrossMark
click for updatesCite this: *J. Mater. Chem. A*, 2015, 3,
19107

A new CO₂-resistant Ruddlesden–Popper oxide with superior oxygen transport: A-site deficient (Pr_{0.9}La_{0.1})_{1.9}(Ni_{0.74}Cu_{0.21}Ga_{0.05})O_{4+δ}

Jian Xue,^a Qing Liao,^c Wei Chen,^b Henny J. M. Bouwmeester,^{*b} Haihui Wang^{*cd} and Armin Feldhoff^{*a}

A-site deficient (Pr_{0.9}La_{0.1})_{1.9}Ni_{0.74}Cu_{0.21}Ga_{0.05}O_{4+δ} ((PL)_{1.9}NCG), with the K₂NiF₄ structure, is found to exhibit higher oxygen transport rates compared with its cation-stoichiometric parent phase. A stable oxygen permeation flux of 4.6 × 10⁻⁷ mol cm⁻² s⁻¹ at 900 °C at a membrane thickness of 0.6 mm is measured, using either helium or pure CO₂ as sweep gas at a flow rate of 30 mL min⁻¹. The oxygen flux is more than two times higher than that observed through A-site stoichiometric (PL)_{2.0}NCG membranes operated under similar conditions. The high oxygen transport rates found for (PL)_{1.9}NCG are attributed to highly mobile oxygen vacancies, compensating A-site deficiency. The high stability against carbonation gives (PL)_{1.9}NCG potential for use, e.g., as a membrane in oxy-fuel combustion processes with CO₂ capture.

Received 7th April 2015
Accepted 9th August 2015

DOI: 10.1039/c5ta02514a

www.rsc.org/MaterialsA

1 Introduction

Clean energy delivery technologies are imperatively required for the purpose of reducing the emission of CO₂ to avert global climate change. Oxygen-transport membranes (OTMs) based on mixed electronic and ionic conductors have gained increasing attention due to their economical, efficient, and environmentally friendly production of oxygen from air and their potential integration in oxy-fuel technologies with CO₂ capture.^{1,2} In the oxy-fuel process, a part of the flue gas, which contains CO₂, is recycled and used as sweep gas. Therefore, oxygen-transport membranes should not only exhibit a high oxygen flux, but also show good stability under CO₂-containing atmospheres.^{3,4}

Acceptor-doped perovskite-type oxides A_{1-x}A'_xB_{1-y}B'_yO_{3-δ} (A, A' = La, Sr, Ba; B, B' = Fe, Co, Nb, etc.) have been investigated extensively as OTMs over the past two decades.^{5,6} The ionic charge carriers created by acceptor-doping are mobile oxygen vacancies. Indeed, high oxygen fluxes are measured for materials with high concentrations of oxygen vacancies. Up to 1/4 of the oxygen sites can be vacant like, for example, SrCo_{0.8}Fe_{0.2}O_{3-δ} and Ba_{0.5}Sr_{0.5}Co_{0.8}Fe_{0.2}O_{3-δ}.^{7,8} A drawback is that these materials are prone to carbonation. An oxygen-impermeable

alkaline-earth carbonate layer will be formed on the membrane surface exposed to the CO₂-containing sweep gas, resulting in a decline of the oxygen permeation flux with time.^{9,10} A-site deficiency is commonly adopted in an attempt to lower the basicity, thereby increasing the resistance of the membrane material towards carbonation.¹¹

Alternatively, problems with limited CO₂ stability could be avoided by the development of alkaline-earth-free membrane materials. In this regard, perovskite-related Ruddlesden–Popper (RP) A_{n+1}B_nO_{3n+1} materials, in particular those with the K₂NiF₄ structure (the first member of the RP oxides with n = 1), are attracting increasing attention.^{12,13} The latter structure consists of alternate AO rock-salt and ABO₃ perovskite-like layers along the crystallographic c-axis, as shown in Fig. 1. Oxygen transport proceeds *via* migration of oxygen interstitials (O3) in the rock-salt layers.^{14,15} Molecular dynamics (MD) simulations predict an interstitialcy diffusion mechanism, also referred to as a 'knock-on' or 'push-pull' mechanism, involving concerted jumps between interstitial oxygen (O3) and apical oxygen (O2) sites, rather than a direct jump between two interstitial sites.¹⁶ A contribution of vacancy-mediated transport may be considered, but this necessitates the formation of oxygen vacancies. Using atomistic computer simulation, Cleave *et al.* predicted that all of the vacancy mechanisms studied in La₂NiO₄ exhibit lower activation energies than the interstitial process.¹⁷ Most reported oxides with the K₂NiF₄ structure are, however, oxygen hyperstoichiometric so that in most of these cases the role of mobile interstitials is predominant.^{12,18}

Using *in situ* high-temperature neutron powder diffraction, Yashima *et al.* provided evidence that indeed the ionic charge carriers in (Pr_{0.9}La_{0.1})_{2.0}Ni_{0.74}Cu_{0.21}Ga_{0.05}O_{4+δ} ((PL)_{2.0}NCG) are oxygen interstitials.^{18,19} It was determined that (PL)_{2.0}NCG

^aInstitute of Physical Chemistry and Electrochemistry, Leibniz University Hannover, Callinstrasse 3A, D-30167 Hannover, Germany. E-mail: armin.feldhoff@pci.uni-hannover.de

^bDepartment of Science and Technology, MESA+ Institute for Nanotechnology, University of Twente, 7500 AE Enschede, The Netherlands. E-mail: h.j.m.bouwmeester@utwente.nl

^cSchool of Chemistry & Chemical Engineering, South China University of Technology, No. 381 Wushan Road, Guangzhou 510640, China. E-mail: hhwang@scut.edu.cn

^dSchool of Chemical Engineering, The University of Adelaide, Adelaide, SA 5005, Australia

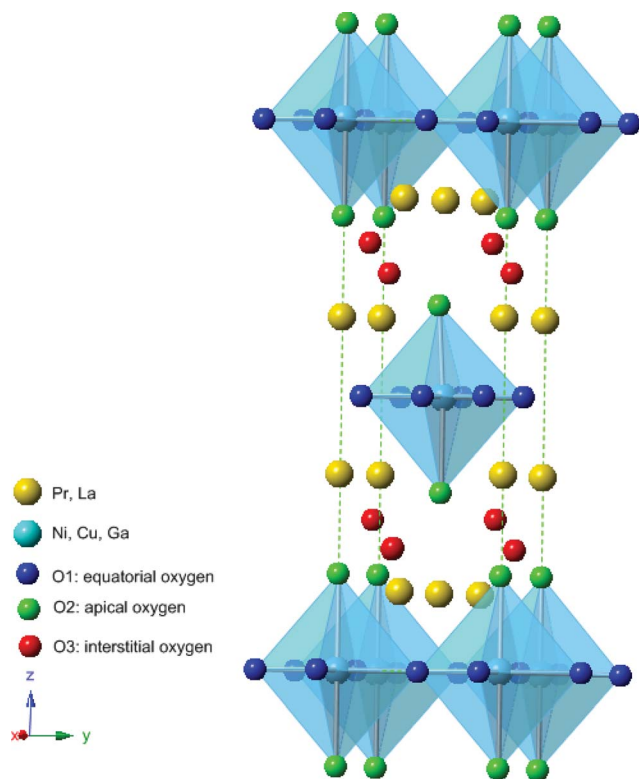


Fig. 1 Oxide with the tetragonal K_2NiF_4 -type structure (space group $I4/mmm$). Atomic positions were calculated from ICSD 173422. For clarity only a subset of the interstitial oxygen ions (O3) is shown.

exhibits specific thermal anisotropic temperature factors expected for migration *via* the interstitialcy mechanism. Interestingly, Ishihara and colleagues found that A-site deficient oxides $Nd_{1.9}(Ni_{0.75}Cu_{0.25})_{0.95}Ga_{0.05}O_4$ and $Pr_{1.9}Ni_{0.75}Cu_{0.25}Ga_{0.05}O_4$ exhibit higher oxygen fluxes than their cation-stoichiometric parent phases.^{20,21} The authors, however, refrained from giving a clear explanation of the role of A-site deficiency in oxygen transport. In this work, we have investigated the influence of A-site deficiency of $(PL)_{2.0}NCG$ on structural parameters, oxygen transport, and stability in CO_2 atmospheres.

2 Experimental

2.1. Preparation

Powders of $(Pr_{0.9}La_{0.1})_{1.9}Ni_{0.74}Cu_{0.21}Ga_{0.05}O_{4+\delta}$ ($(PL)_{1.9}NCG$) and $(PL)_{2.0}NCG$ were prepared by a combined citrate and ethylenediamine-tetraacetic-acid (EDTA) method as described previously.^{22,23} The as-prepared powders were uniaxially pressed at 20 MPa to obtain green pellets followed by their sintering in air at 1230 °C for 10 h in a bed of the corresponding powder. The density of the sintered disk membranes obtained was measured by the Archimedes method using distilled water. Only membranes with a relative density higher than 95% were selected for permeation experiments. The membranes were polished to the desired thickness using 1200 grit-sandpaper and then washed with ethanol.

2.2. Structural characterization

The crystal structure of the sintered disks was studied by using an *in situ* X-ray diffractometer (XRD, D8 Advance, Bruker-AXS, with $Cu K\alpha$ radiation) equipped with a HTK-1200N high-temperature oven chamber (Anton-Paar). Measurements were conducted under a CO_2 atmosphere from 30 to 1000 °C. The temperature was step-wise increased, with a dwell time at each step of 50 min before actual data collection. The oxygen content of $(PL)_{1.9}NCG$ and $(PL)_{2.0}NCG$ in air at 900 °C was evaluated by hydrogen reduction in a thermogravimetric (TGA) apparatus (Netzsch TG 449 F3), assuming that the products of hydrogen reduction were Pr_2O_3 , La_2O_3 , Ni, Cu and Ga.^{12,24} The microstructure of the disk membrane was examined by scanning electron microscopy (SEM) using a JEOL JSM-6700F field-emission instrument operating at an excitation voltage of 2 kV. The elemental composition of the membrane was determined by energy dispersive X-ray spectroscopy (EDXS), using an Oxford Instruments INCA-300 EDX spectrometer with an ultrathin window and at an excitation voltage of 20 kV.

2.3. Oxygen permeation experiments

The oxygen flux through the membranes with different thicknesses was investigated in the range of 800–975 °C using a home-made high-temperature oxygen permeation cell, which is described in detail elsewhere.^{25,26} A commercial ceramic sealant (Huitian, Hubei, China) was used to seal the disk-shaped membrane onto an alumina tube. Synthetic air was fed ($150 mL min^{-1}$) to the feed side of the membrane, while He or CO_2 gas was fed to the sweep side. Unless specified otherwise a sweep gas flow rate of $30 mL min^{-1}$ was maintained. Gas flow rates were calibrated with a soap bubble flow meter. The composition of the effluent was analyzed by on-line gas chromatography (GC, Agilent Technologies, 7890A). The leakage of oxygen was subtracted in the calculation of the oxygen flux.^{25,27} The contribution of leakage to the apparent oxygen flux was below 0.5% in all cases.

3 Results and discussion

3.1. Phase analysis and microstructure

Fig. 2 shows the XRD patterns of $(PL)_{1.9}NCG$ and $(PL)_{2.0}NCG$ ceramics after sintering at 1230 °C for 10 h in air. Analysis of the patterns confirms that both materials adopt the tetragonal K_2NiF_4 structure (ICDD PDF number: 01-087-1679). No impurity phases are detected.^{28,29} For a more precise evaluation of the influence of A-site deficiency on the XRD pattern, the reflections at 31.6°, 69° and 79° are magnified and compared in Fig. 2b–d, respectively. The 113 reflection of $(PL)_{1.9}NCG$ at 31.6° is slightly shifted to higher 2θ values compared to that of $(PL)_{2.0}NCG$ as shown in Fig. 2b. The 324 and 400 reflections are shifted to a higher angle and merge with the 208 reflection, which is shifted to a lower angle, as shown in Fig. 2c. A similar phenomenon is found around 79° as shown in Fig. 2d, where the 414 and 420 reflections are found to be merged with the 228 reflection. These observations are consistent with the different lattice parameters of $(PL)_{1.9}NCG$ and $(PL)_{2.0}NCG$, which are reported in Table 1.

In situ XRD measurements were performed on (PL)_{1.9}NCG under a pure CO₂ atmosphere from room temperature to 1000 °C. As seen from Fig. 3, no additional reflections are found that would indicate the presence or formation of other phases, e.g., carbonates. The results are consistent with those from our previous study, in which it was found that (PL)_{2.0}NCG also possesses excellent chemical stability under CO₂ atmospheres.^{29,30}

SEM micrographs of the (PL)_{1.9}NCG and (PL)_{2.0}NCG membranes, which were sintered at 1230 °C for 10 h in air, are presented in Fig. 4. As seen from this figure, both membranes show high density. The average grain area estimated from the micrographs is about 51 μm² for (PL)_{1.9}NCG, which is slightly higher than the value of 42 μm² found for (PL)_{2.0}NCG. Some fine-grained furnace dust particles are seen in both SEM micrographs. These could be successfully removed by polishing the membranes prior to permeation measurements as was revealed from SEM micrographs recorded after the polishing procedure.

Table 1 lists various properties of (PL)_{1.9}NCG and (PL)_{2.0}NCG. The unit cell parameters of both materials are close. Compared to (PL)_{2.0}NCG, the lattice of (PL)_{1.9}NCG has shrunk slightly in the *c*-axis direction and has expanded slightly in the *a*-*b* plane.^{31,32} Furthermore, (PL)_{1.9}NCG shows a higher relative

density, which might indicate that A-site deficiency enhances the sintering process.³³ The average thermal expansion coefficient of (PL)_{1.9}NCG under a CO₂ atmosphere is 15.9 × 10⁻⁶ K⁻¹, which is slightly higher than the value of 15.1 × 10⁻⁶ K⁻¹ observed for (PL)_{2.0}NCG under the same conditions.³⁰ Note further that the oxygen content of A-site deficient (PL)_{1.9}NCG, at 900 °C in air, is significantly less than that observed for A-site stoichiometric (PL)_{2.0}NCG. The latter suggests that A-site deficiency is mainly compensated by the removal of oxygen from the lattice.

3.2. Oxygen flux

An Arrhenius plot of the oxygen flux through a (PL)_{1.9}NCG membrane with a thickness of 0.6 mm is shown in Fig. 5. Also included are data of oxygen permeation for (PL)_{2.0}NCG from our previous study.²⁹ Similar oxygen fluxes are found whether using He or CO₂ as sweep gas, albeit at the lowest temperatures the measured oxygen flux using CO₂ as sweep gas tends to be slightly lower. The latter may be attributed to the adsorption of CO₂ molecules at the surface, thereby blocking the surface exchange reaction.^{29,34} Compared to (PL)_{2.0}NCG, slightly lower activation energies are found for A-site deficient (PL)_{1.9}NCG. Apparent activation energies in the temperature range of 800–975 °C, using He as sweep gas, are 25 and 27 kJ mol⁻¹ for (PL)_{1.9}NCG and (PL)_{2.0}NCG, respectively. At 900 °C, the oxygen flux through (PL)_{1.9}NCG is 4.6 × 10⁻⁷ mol cm⁻² s⁻¹ irrespective of the use of CO₂ or He as sweep gas. The observed oxygen flux is more than two times higher than the value of 1.9 × 10⁻⁷ mol cm⁻² s⁻¹ observed for (PL)_{2.0}NCG under the same conditions.²⁹ A-site cation deficiency thus has a large influence on the oxygen permeability.

The oxygen flux was further investigated as a function of membrane thickness. Oxygen permeation through dense mixed-conducting oxide membranes is governed by bulk diffusion and surface exchange. If bulk diffusion is the rate limiting step, the flux can be described by the Wagner equation,^{5,35}

$$jO_2 = -\frac{RT}{4F^2L} \frac{\sigma_e \sigma_i}{\sigma_e + \sigma_i} \ln \frac{pO'_2}{pO''_2} \quad (1)$$

where jO_2 , R , F , T , L , σ_e , and σ_i denote the oxygen flux, gas constant, Faraday constant, temperature, membrane thickness, and the partial electronic and ionic conductivity, respectively. pO'_2 is the oxygen partial pressure maintained at the feed side, while pO''_2 is the oxygen partial pressure at the sweep side. Hence, if the oxygen flux is entirely governed by bulk diffusion, the plot of the normalized oxygen flux $jO_2/\ln(pO'_2/pO''_2)$ versus reciprocal thickness ($1/L$) should be linear with the line intersecting the origin. Fig. 6 shows that the normalized oxygen fluxes for both (PL)_{1.9}NCG and (PL)_{2.0}NCG increase proportionally with $1/L$ for thicknesses greater than approximately 1.6 mm ($1/L = 0.635 \text{ mm}^{-1}$), but depart from a linear relationship for smaller thicknesses. These results reveal that the oxygen flux is predominantly limited by bulk diffusion for a membrane thickness greater than ~1.6 mm and by surface exchange for smaller thicknesses.

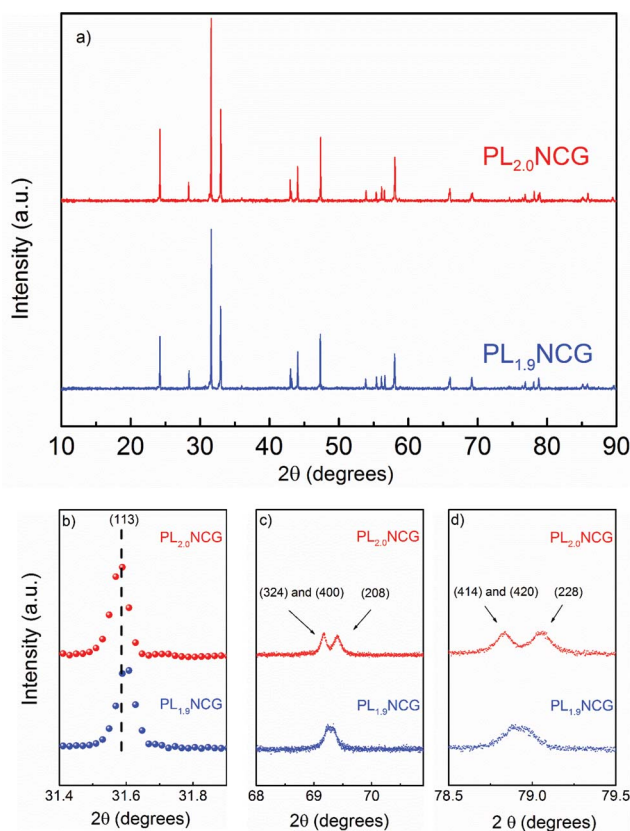


Fig. 2 (a) XRD patterns of (PL)_{1.9}NCG and (PL)_{2.0}NCG after sintering at 1230 °C for 10 h in air, and (b) magnifications of selected regions of the patterns shown in (a).

Table 1 Various parameters of (PL)_{1.9}NCG and (PL)_{2.0}NCG. Values between parentheses are standard deviations. Experimental data were acquired from sintered ceramics or powder obtained from crushed ceramics

| | ρ_{exp} g cm ⁻³ | $\rho_{\text{exp}}/\rho_{\text{theo}}$ % | Average grain size (μm^2) | Crystal symmetry (space group) | Cell parameters (\AA) | Average thermal expansion coefficients in 30 °C–1000 °C under CO ₂ (10^{-6} K ⁻¹) | Oxygen content at 900 °C in air |
|-------------------------|---|---|--|--------------------------------------|--|---|------------------------------------|
| (PL) _{2.0} NCG | 7.51(5) | 96(1) | 42(2) | Tetragonal <i>I4/mmm</i> | $a = b = 3.8305(4)$, $c = 12.5600(20)$ | 15.1 (ref. 30) | 4.25(2) |
| (PL) _{1.9} NCG | 7.40(5) | 98(1) | 50(2) | Tetragonal <i>I4/mmm</i> | $a = b = 3.8345(4)$, $c = 12.5547(20)$ | 15.9(6) | 3.98(2) |

Since in both (PL)_{1.9}NCG and (PL)_{2.0}NCG the electronic conductivity predominates over the ionic conductivity, eqn (1) can be simplified to

$$j_{\text{O}_2} = -\frac{RT}{4^2 F^2 L} \sigma_i \ln \frac{p_{\text{O}_2}'}{p_{\text{O}_2}''} \quad (2)$$

Using this equation, the ionic conductivity was calculated from the data of oxygen permeation measurements obtained for 2.3 mm thick membranes. At 900 °C, a value of 0.21 S cm⁻¹ is found for A-site deficient (PL)_{1.9}NCG, to be compared with 0.10 S cm⁻¹ found for A-site stoichiometric (PL)_{2.0}NCG. Increasing the sweep gas flow rate increases the oxygen partial pressure gradient across the membrane. Fig. 7 shows that the oxygen flux measured through a 0.6 mm thick membrane of (PL)_{1.9}NCG at different temperatures increases upon increasing the flow rate of the He sweep gas.

3.3. Stability under CO₂

High oxygen flux and good chemical stability are two key factors for industrial application of oxygen transport membranes. Good CO₂ resistance was found for the A-site stoichiometric (PL)_{2.0}NCG.²⁹ To assess the stability of A-site deficient (PL)_{1.9}NCG against carbonation, the oxygen permeation performance was studied by periodically changing the sweep gas between He and CO₂. As can be seen from Fig. 8, only a marginal, reversible change of the oxygen flux occurs

when the sweep gas is switched back and forth between He and CO₂. Fig. 9 shows the long-term oxygen permeation behavior of the (PL)_{1.9}NCG membrane at 900 and 975 °C, using either He or pure CO₂ as sweep gas. Stable oxygen fluxes with no sign of deterioration are observed over 200 h. Comparing the XRD patterns of the (PL)_{1.9}NCG membrane before and after the long-term permeation tests revealed no formation of second phases, as shown in Fig. 10. In particular, no evidence of carbonation formation was found. Fig. 11 depicts SEM/EDXS images of a cross-section of the (PL)_{1.9}NCG membrane after the oxygen permeation tests. The results confirm a homogeneous distribution of all elements. The observations confirm the excellent stability of (PL)_{1.9}NCG under a CO₂ atmosphere. The observed behavior is in marked contrast with many earth-alkaline containing perovskite oxides whose oxygen permeation fluxes are found to decrease sharply upon CO₂ exposure.^{9,10}

3.4. Influence of A-site deficiency on oxygen transport

Data from this study demonstrate that A-site deficient (PL)_{1.9}NCG shows superior oxygen transport properties compared to A-site stoichiometric (PL)_{2.0}NCG. As was mentioned in the introduction, similar observations have been reported by Ishihara and colleagues for A-site deficient Nd_{1.9}(Ni_{0.75}Cu_{0.25})_{0.95}Ga_{0.05}O₄ and Pr_{1.9}Ni_{0.75}Cu_{0.25}Ga_{0.05}O₄ compared to their A-site stoichiometric forms.^{20,21} The latter

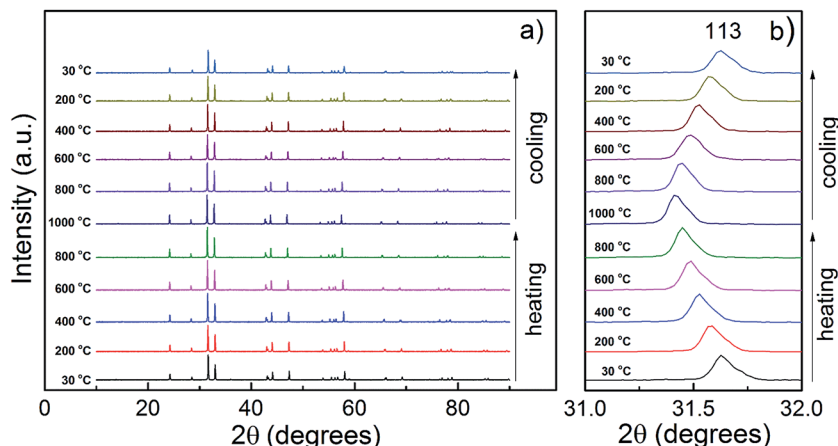


Fig. 3 (a) *In-situ* high-temperature XRD patterns of calcined (PL)_{1.9}NCG powder collected during exposure to pure CO₂, and (b) magnified view of the (113) reflection. Diffractograms were recorded in intervals of 100 °C while not all are displayed for clarity reasons.

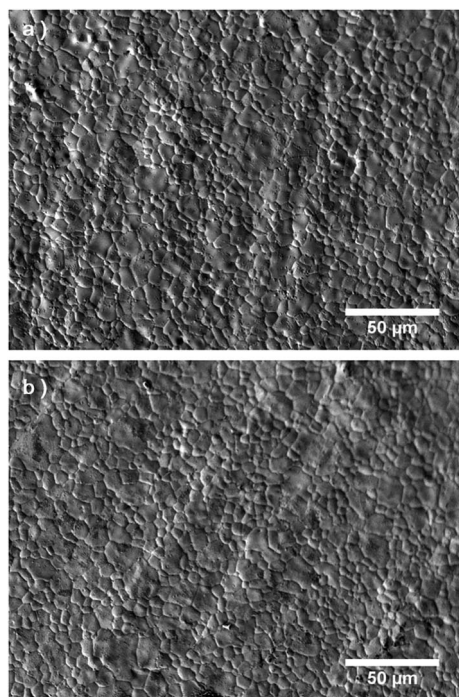


Fig. 4 Surface SEM micrographs of sintered (a) $(\text{PL})_{2.0}\text{NCG}$ and (b) $(\text{PL})_{1.9}\text{NCG}$ membranes.

authors attributed the phenomenon to grain size effects, increased concentration of interstitial oxygen, or enhanced diffusivity of interstitial oxygen.^{20,21,36} It may be noted that the grain sizes found in this study for $(\text{PL})_{1.9}\text{NCG}$ and $(\text{PL})_{2.0}\text{NCG}$ are similar (see Fig. 4), while the oxygen hyperstoichiometry decreases rather than increases by introducing A-site deficiency

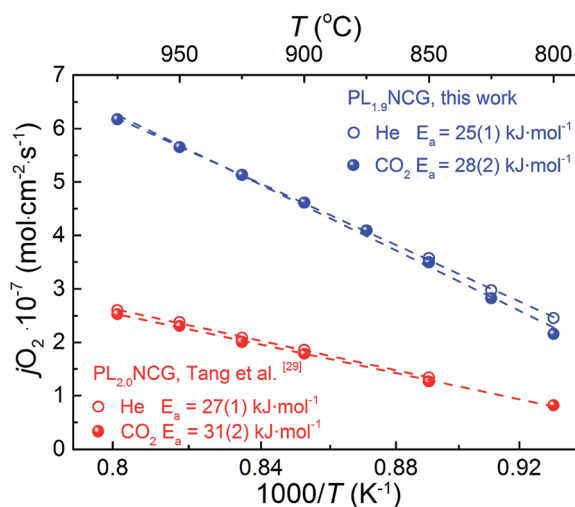


Fig. 5 Temperature dependence of the oxygen permeation flux for $(\text{PL})_{1.9}\text{NCG}$ and $(\text{PL})_{2.0}\text{NCG}$, measured using different sweep gases. Data for both materials were collected under similar conditions. The membrane thicknesses are 0.6 mm. Data for $(\text{PL})_{2.0}\text{NCG}$ were taken from our previous study.²⁹ Apparent activation energies are listed in the figure.

(see Table 1). Clearly other factors must be taken into to account for the observations.

Hydrogen reduction experiments show that, at 900 °C, $(\text{PL})_{2.0}\text{NCG}$ is hyperstoichiometric with $4 + \delta = 4.25$, while $(\text{PL})_{1.9}\text{NCG}$ is found to be almost oxygen stoichiometric, $4 + \delta = 3.98$ (Table 1). At the same time the oxygen fluxes through $(\text{PL})_{1.9}\text{NCG}$ membranes, in the range of 800–975 °C, exceed those through $(\text{PL})_{2.0}\text{NCG}$ membranes by a factor of 2–3 (Fig. 5). Interestingly, despite the apparent lowering in the ionic charge carrier concentration by introducing A-site deficiency, oxygen transport has increased. The results are taken as evidence that the ionic charge carriers in $(\text{PL})_{1.9}\text{NCG}$ must exhibit a higher diffusivity that overcompensates the loss in the ionic charge carrier concentration compared to those in $(\text{PL})_{2.0}\text{NCG}$. As the oxygen content of $(\text{PL})_{1.9}\text{NCG}$ is found to be almost stoichiometric, the role of oxygen vacancy diffusion becomes significant. Accordingly, the enhanced oxygen transport observed for $(\text{PL})_{1.9}\text{NCG}$ can be accounted for by fast oxygen transport *via* a vacancy mechanism. Such a conclusion would be consistent with the finding by Cleave *et al.* that the most likely pathway for oxygen migration in La_2NiO_4 , *i.e.*, with the lowest activation energy, is a vacancy mechanism, involving transfer between two apical (O2) sites.¹⁷

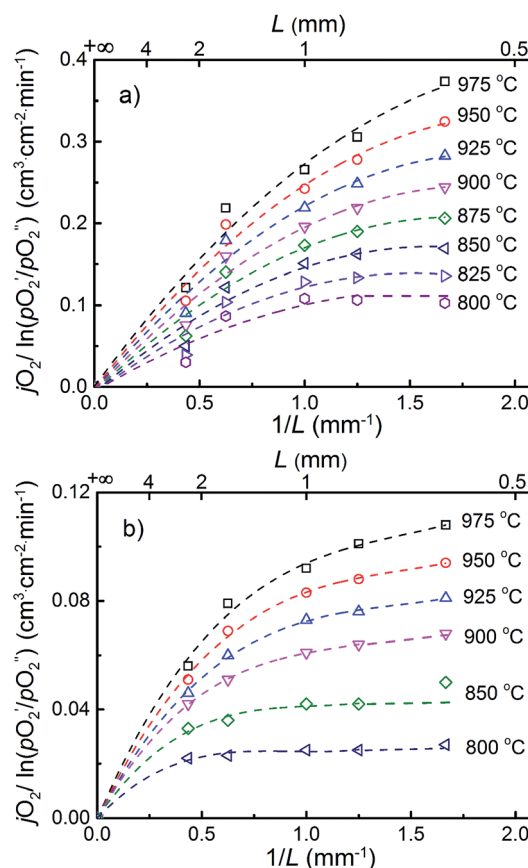


Fig. 6 Dependence of the normalized oxygen flux on the inverse membrane thickness for (a) $(\text{PL})_{1.9}\text{NCG}$ and (b) $(\text{PL})_{2.0}\text{NCG}$. Data for the latter were taken from our previous study.²⁹ Note the different vertical scales.

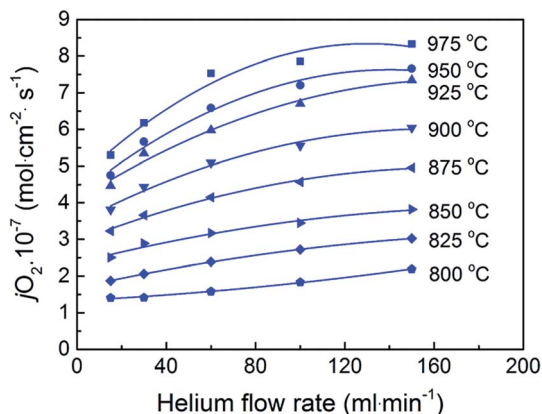
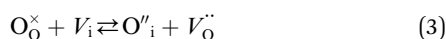


Fig. 7 Dependence of the oxygen flux through a 0.6 mm thick (PL)_{1.9}NCG membrane at different temperatures on the He sweep gas flow rate.

The role of a vacancy mechanism in overall oxygen transport in (PL)_{1.9}NCG can be illustrated by simple defect chemical considerations. The concentration of oxygen vacancies is determined by anion Frenkel disorder. Using the standard Kröger–Vink defect notation, this equilibrium can be expressed as



Close to stoichiometric conditions, *i.e.*, in the regime for dilute defect concentrations, and ignoring defect association, the anti-Frenkel equilibrium constant K_{AF} can be presented as

$$K_{\text{AF}} \approx [\text{O}'_\text{i}][V''_\text{O}] \approx \delta_\text{i} \cdot \delta_\text{v} \quad (4)$$

where δ_i and δ_v are the molar fractions of oxygen interstitials and oxygen vacancies, respectively. The overall non-stoichiometry parameter is given by $\delta = \delta_\text{i} - \delta_\text{v}$. Eqn (4) can be used to calculate δ_i and δ_v provided that K_{AF} is known. Data of such calculation, assuming $K_{\text{AF}} = 10^{-2}$, are shown in Fig. 12.

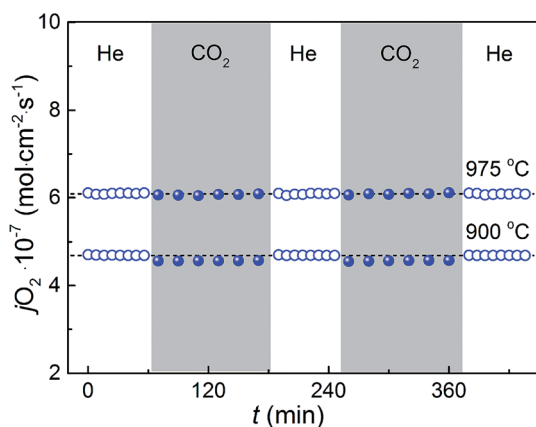


Fig. 8 Oxygen permeation flux through a 0.6 mm thick (PL)_{1.9}NCG membrane at 900 and 975 °C. Data were collected by periodically changing the sweep gas between He and CO₂. Horizontal dashed lines are guides to the eye.

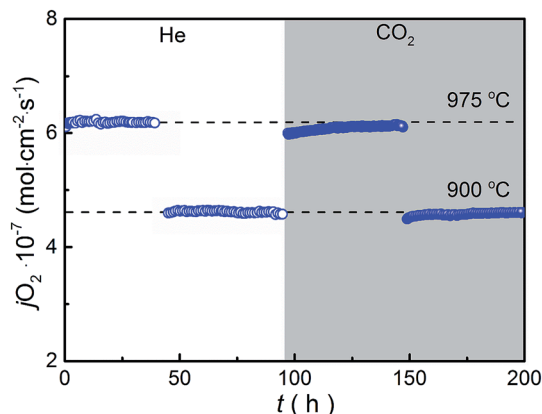


Fig. 9 Long-term stability test of the oxygen permeation flux through a 0.6 mm thick (PL)_{1.9}NCG membrane. Data were collected at two different temperatures, using He and CO₂ as sweep gases as indicated in the figure. Horizontal dashed lines are guides to the eye.

The Nernst–Einstein equation can be used to express the ionic conductivity in terms of the defect concentrations and their diffusivities,

$$\sigma_\text{i} = \frac{4F^2}{RTV_\text{m}} (\delta_\text{i}D_\text{i} + \delta_\text{v}D_\text{v}) \quad (5)$$

Where V_m is the molar volume, and D_i and D_v are the diffusivities of interstitials and vacancies, respectively. Eqn (5) can be rewritten into,

$$\sigma_\text{i} = \frac{4F^2}{RTV_\text{m}} D_\text{i} (\delta_\text{i} + \delta_\text{v}\xi) \quad (6)$$

where we defined the parameter $\xi = D_\text{v}/D_\text{i}$. The relative magnitudes of the diffusivities affect the overall ionic conductivity, as is illustrated in Fig. 13. If the defect diffusivities are equal ($\xi = 1$), the ionic conductivity is at minimum at the stoichiometric composition ($\delta = 0$). The plot of the ionic conductivity *versus* δ obtained for $\xi = 1$ is symmetrical about $\delta = 0$. With increasing ξ , the minimum shifts to higher δ values. In this case, a higher ionic conductivity is obtained for hypostoichiometric ($\delta < 0$) than for hyperstoichiometric ($\delta > 0$) compositions of a similar

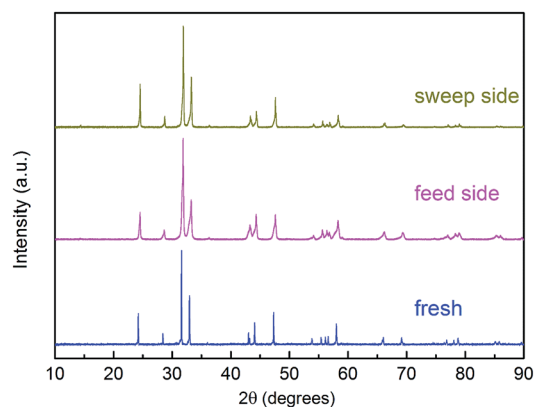


Fig. 10 XRD patterns of fresh and spent (PL)_{1.9}NCG membranes after long-term oxygen permeation tests.

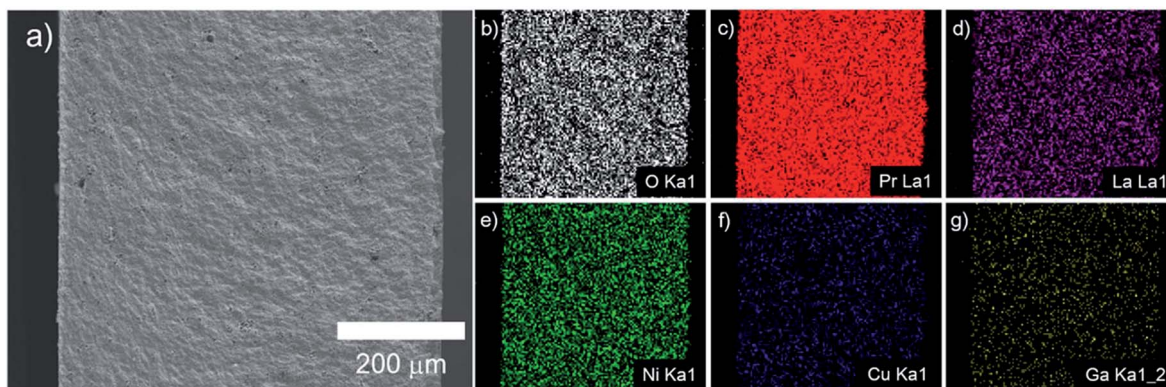


Fig. 11 (a) SEM, and (b–g) EDXS images of a cross-section of the $(\text{PL})_{1.9}\text{NCG}$ membrane after the long-term permeation tests.

absolute magnitude. It should be emphasized that the value obtained for ξ is determined by the value of K_{AF} . It is easily demonstrated by calculation that, at given value of $K_{\text{AF}} = 10^{-2}$, ξ must be 10 to yield a two times higher ionic conductivity for $(\text{PL})_{1.9}\text{NCG}$, with $\delta = -0.02$, than for $(\text{PL})_{2.0}\text{NCG}$, with $\delta = 0.25$, as is experimentally observed (see Table 1).

In the A_2BO_4 oxides (with the K_2NiF_4 structure), the interstitial oxygen ions O_3 are in a tetrahedral environment of the A-site cations as well as of the apical oxygen O_2 .¹⁵ MD simulations show only a weak dependence of the diffusivity of oxygen interstitials in $\text{Pr}_2\text{NiO}_{4+\delta}$ with the degree of oxygen hyperstoichiometry.³⁷ The observations are consistent with MD simulations of oxygen transport in $\text{La}_2\text{NiO}_{4+\delta}$.¹⁶ Several researchers have investigated the effect of acceptor-doping on the oxygen diffusivity in oxides with the K_2NiF_4 structure. Acceptor doping reduces the concentration of oxygen interstitials. The corresponding results of ^{18}O tracer diffusion studies by secondary-ion mass spectroscopy (SIMS) show the oxygen diffusivities in $\text{La}_{2-x}\text{Sr}_x\text{NiO}_{4+\delta}$ and

$\text{La}_{2-x}\text{Sr}_x\text{CuO}_{4+\delta}$ to be suppressed by several orders of magnitudes below the diffusivities for the undoped materials.^{12,38–41} For small Sr addition, the observations are explained by the concomitant decrease in the concentration of oxygen interstitials.^{12,41} For the higher Sr addition ($x \leq 0.2$), where charge compensation of the acceptor dopant occurs, in part, by the formation of oxygen vacancies, these are explained by the occurrence of defect associates $V_{\text{O}}^{\bullet\bullet} - \text{Sr}'_{\text{La}}$, or vacancy ordering, due to the electrostatic interactions between oppositely charged oxygen vacancies and dopant cations. These findings are in apparent contrast with those from the present work. Assuming that, on the introduction of A-site deficiency, A-site cation vacancies ($V_{\text{pr}}^{\bullet\bullet}$) and oxygen vacancies are formed, defect associates in $(\text{PL})_{1.9}\text{NCG}$ are likely on the basis of simple charge considerations. The high oxygen transport rates observed in $(\text{PL})_{1.9}\text{NCG}$, however, provide no evidence of their detrimental influence on ionic conductivity. Our results are believed to have general relevance for optimizing

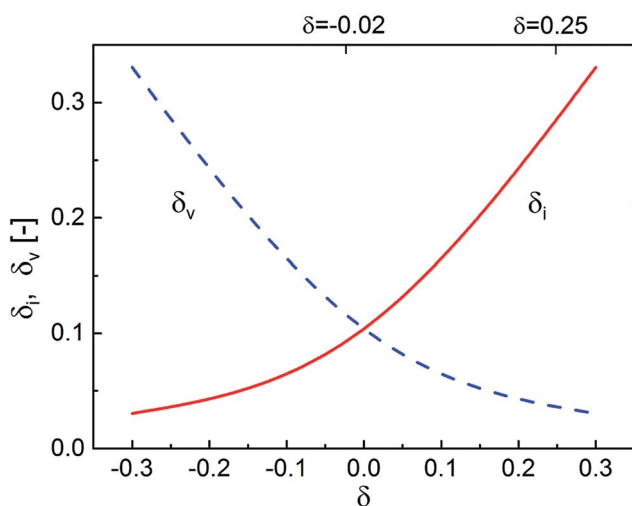


Fig. 12 Concentration of interstitial oxygen ions (δ_i) and oxygen vacancies (δ_v) as a function of the overall nonstoichiometry parameter $\delta = \delta_i - \delta_v$, calculated using eqn (4), assuming $K_{\text{AF}} = 10^{-2}$. Values of δ , which are indicated on the top scale, refer to $(\text{PL})_{1.9}\text{NCG}$ and $(\text{PL})_{2.0}\text{NCG}$ (see Table 1).

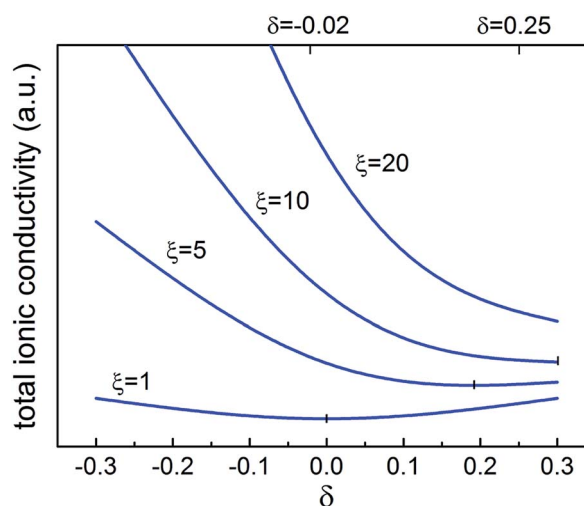


Fig. 13 The influence of oxygen nonstoichiometry on the apparent ionic conductivity calculated for different values of the oxygen vacancy/oxygen interstitial diffusivity ratio $\xi = D_v/D_i$. Values of δ , which are indicated on the top scale, refer to $(\text{PL})_{1.9}\text{NCG}$ and $(\text{PL})_{2.0}\text{NCG}$ (see Table 1).

the ionic conductivity of A_2BO_4 oxides by tuning the A/B-site stoichiometry.

4 Conclusion

(PL)_{1.9}NCG has been studied with a view to determine the effects of A-site deficiency on structural parameters, oxygen transport and stability under CO₂ atmospheres. (PL)_{1.9}NCG is found to exhibit higher oxygen transport rates compared with its cation stoichiometric parent phase. The high oxygen transport rates are attributed to highly mobile oxygen vacancies and charge compensating cationic vacancies. The high structural stability towards carbonation gives (PL)_{1.9}NCG potential for use as a membrane, e.g., in oxy-fuel combustion processes with CO₂ capture. As exemplified in this work, the concept of A-deficiency can be used to optimize oxygen transport in layered A_2BO_4 oxides (with the K₂NiF₄ structure).

Acknowledgements

J. X. acknowledges financial support from the China Scholarship Council (CSC), National Science Fund for Distinguished Young Scholars of China (No. 21225625) and the Australian Research Council (ARC) through the Future Fellow Program (FT140100757). Financial support from the German Research Foundation (DFG) (No. FE928/7-1) is appreciated. The authors also greatly acknowledge O. Ravkina, A. Schulz and F. Steinbach for technical support.

Notes and references

- J. D. Figueroa, T. Fout, S. Plasynski, H. McIlvried and R. D. Srivastava, *Int. J. Greenhouse Gas Control*, 2008, **2**, 9–20.
- C. Gough, *Int. J. Greenhouse Gas Control*, 2008, **2**, 155–168.
- R. Kneer, D. Toporov, M. Förster, D. Christ, C. Broeckmann, E. Pfaff, M. Zwick, S. Engels and M. Modigell, *Energy Environ. Sci.*, 2010, **3**, 198–207.
- X. Tan, K. Li, A. Thursfield and I. S. Metcalfe, *Catal. Today*, 2008, **131**, 292–304.
- J. Sunarso, S. Baumann, J. M. Serra, W. A. Meulenber, S. Liu, Y. S. Lin and J. C. Diniz da Costa, *J. Membr. Sci.*, 2008, **320**, 13–41.
- K. Zhang, J. Sunarso, Z. Shao, W. Zhou, C. Sun, S. Wang and S. Liu, *RSC Adv.*, 2011, **1**, 1661–1676.
- L. Qiu, T. H. Lee, L. M. Liu, Y. L. Yang and A. J. Jacobson, *Solid State Ionics*, 1995, **76**, 321–329.
- Z. Shao, W. Yang, Y. Cong, H. Dong, J. Tong and G. Xiong, *J. Membr. Sci.*, 2000, **172**, 177–188.
- M. Arnold, H. Wang and A. Feldhoff, *J. Membr. Sci.*, 2007, **293**, 44–52.
- J. Yi, M. Schroeder, T. Weirich and J. Mayer, *Chem. Mater.*, 2010, **22**, 6246–6253.
- V. Kharton, A. Kovalevsky, E. Tsipis, A. Viskup, E. Naumovich, J. Jurado and J. Frade, *J. Solid State Electrochem.*, 2002, **7**, 30–36.
- E. Boehm, J. Bassat, P. Dordor, F. Mauvy, J. Grenier and P. Stevens, *Solid State Ionics*, 2005, **176**, 2717–2725.
- M. Yashima, *J. Ceram. Soc. Jpn.*, 2009, **117**, 1055–1059.
- J. M. Bassat, P. Odier, A. Villesuzanne, C. Marin and M. Pouchard, *Solid State Ionics*, 2004, **167**, 341–347.
- L. Minervini, R. W. Grimes, J. A. Kilner and K. E. Sickafus, *J. Mater. Chem.*, 2000, **10**, 2349–2354.
- A. Chronos, D. Parfitt, J. A. Kilner and R. W. Grimes, *J. Mater. Chem.*, 2010, **20**, 266.
- A. R. Cleave, J. A. Kilner, S. J. Skinner, S. T. Murphy and R. W. Grimes, *Solid State Ionics*, 2008, **179**, 823–826.
- M. Yashima, H. Yamada, S. Nuansaeng and T. Ishihara, *Chem. Mater.*, 2012, **24**, 4100–4113.
- M. Yashima, M. Enoki, T. Wakita, R. Ali, Y. Matsushita, F. Izumi and T. Ishihara, *J. Am. Chem. Soc.*, 2008, **130**, 2762–2763.
- T. Ishihara, N. Sirikanda, K. Nakashima, S. Miyoshi and H. Matsumoto, *J. Electrochem. Soc.*, 2010, **157**, B141.
- A. Kawahara and T. Ishihara, *Electrochem. Solid-State Lett.*, 2010, **13**, B76.
- A. Feldhoff, M. Arnold, J. Martynczuk, T. M. Gesing and H. Wang, *Solid State Sci.*, 2008, **10**, 689–701.
- J. Xue, Q. Liao, Y. Wei, Z. Li and H. Wang, *J. Membr. Sci.*, 2013, **443**, 124–130.
- W. Chen, A. Nijmeijer and L. Winnubst, *Solid State Ionics*, 2012, **229**, 54–58.
- H. Luo, B. Tian, Y. Wei, H. Wang, H. Jiang and J. Caro, *AIChE J.*, 2010, **56**, 604–610.
- J. Xue, Q. Zheng, Y. Wei, K. Yuan, Z. Li and H. Wang, *Ind. Eng. Chem. Res.*, 2012, **51**, 4703–4709.
- H. Wang, R. Wang, D. T. Liang and W. Yang, *J. Membr. Sci.*, 2004, **243**, 405–415.
- C. Tablet, G. Grubert, H. Wang, T. Schiestel, M. Schroeder, B. Langanke and J. Caro, *Catal. Today*, 2005, **104**, 126–130.
- J. Tang, Y. Wei, L. Zhou, Z. Li and H. Wang, *AIChE J.*, 2012, **58**, 2473–2478.
- Y. Wei, O. Ravkina, T. Klande, H. Wang and A. Feldhoff, *J. Membr. Sci.*, 2013, **429**, 147–154.
- W. Cheikh-Rouhou Koubaa, M. Koubaa, A. Cheikh-Rouhou, W. Boujelben and A. M. Haghiri-Gosnet, *J. Alloys Compd.*, 2008, **455**, 67–72.
- W. Zhou, R. Ran, Z. Shao, W. Jin and N. Xu, *J. Power Sources*, 2008, **182**, 24–31.
- K. Shan and X.-M. Guo, *Mater. Lett.*, 2013, **113**, 126–129.
- X. Tan, N. Liu, B. Meng, J. Sunarso, K. Zhang and S. Liu, *J. Membr. Sci.*, 2012, **389**, 216–222.
- C. Wagner, *Z. Phys. Chem. B*, 1933, **21**, 25–41.
- S. Miyoshi, T. Furuno, O. Sangoanruang, H. Matsumoto and T. Ishihara, *J. Electrochem. Soc.*, 2007, **154**, B57.
- D. Parfitt, A. Chronos, J. A. Kilner and R. W. Grimes, *Phys. Chem. Chem. Phys.*, 2010, **12**, 6834–6836.
- Z. Li, R. Haugsrud and T. Norby, *Solid State Ionics*, 2011, **184**, 42–46.
- E. J. Opila, H. L. Tuller, B. J. Wuensch and J. Maier, *J. Am. Ceram. Soc.*, 1993, **76**, 2363–2369.
- J. Routbort, S. Rothman, B. Flandermeyer, L. Nowicki and J. Baker, *J. Mater. Res.*, 1988, **3**, 116–121.
- S. J. Skinner and J. A. Kilner, *Solid State Ionics*, 2000, **135**, 709–712.